UCSF
UC San Francisco Previously Published Works

Title

Unsupervised Learning of Spatiotemporal Interictal Discharges in Focal Epilepsy

Permalink

https://escholarship.org/uc/item/0gq3p3pr

Journal

Neurosurgery, 83(4)

ISSN

0148-396X

Authors

Baud, Maxime O
Kleen, Jonathan K
Anumanchipalli, Gopala K
et al.

Publication Date

2018-10-01

DOI

10.1093/neuros/nyx480

Peer reviewed

Unsupervised Learning of Spatiotemporal Interictal Discharges in Focal Epilepsy

Maxime O. Baud, MD, PhD[*‡]
Jonathan K. Kleen, MD, PhD[‡]
Gopala K. Anumanchipalli, PhD[*]
Liberty S. Hamilton, PhD[*]
Yee-Leng Tan, MRCP[‡¶]
Robert Knowlton, MD[‡]
Edward F. Chang, MD[*]

*Department of Neurological surgery, University of California, San Francisco, California; ‡Department of Neurology, University of California, San Francisco, California; ¶National Neuroscience Institute, Singapore, Singapore

Correspondence:
Edward F. Chang, MD,
Department of Neurological Surgery and Department of Physiology,
University of California, San Francisco,
675 Nelson Rising Lane, Room 511,
San Francisco, CA 94158.
E-mail: edward.chang@ucsf.edu

BACKGROUND: Interictal epileptiform discharges are an important biomarker for localization of focal epilepsy, especially in patients who undergo chronic intracranial monitoring. Manual detection of these pathophysiological events is cumbersome, but is still superior to current rule-based approaches in most automated algorithms.

OBJECTIVE: To develop an unsupervised machine-learning algorithm for the improved, automated detection and localization of interictal epileptiform discharges based on spatiotemporal pattern recognition.

METHODS: We decomposed 24 h of intracranial electroencephalography signals into basis functions and activation vectors using non-negative matrix factorization (NNMF). Thresholding the activation vector and the basis function of interest detected interictal epileptiform discharges in time and space (specific electrodes), respectively. We used convolutive NNMF, a refined algorithm, to add a temporal dimension to basis functions.

RESULTS: The receiver operating characteristics for NNMF-based detection are close to the gold standard of human visual-based detection and superior to currently available alternative automated approaches (93% sensitivity and 97% specificity). The algorithm successfully identified thousands of interictal epileptiform discharges across a full day of neurophysiological recording and accurately summarized their localization into a single map. Adding a temporal window allowed for visualization of the archetypal propagation network of these epileptiform discharges.

CONCLUSION: Unsupervised learning offers a powerful approach towards automated identification of recurrent pathological neurophysiological signals, which may have important implications for precise, quantitative, and individualized evaluation of focal epilepsy.

KEY WORDS: Epileptogenic tissue, Interictal epileptiform discharges, Automated detection, Non-negative matrix factorization, Intracranial monitoring

Interictal epileptiform discharges (IEDs) are a hallmark of the epileptic brain, and their localization is a critical complement to definitive delineation of the seizure onset zone for optimal treatment. IEDs include spikes (or sharp waves) and high-frequency oscillations (HFOs)

ABBREVIATIONS: BFs, basis functions; **EEG,** electroencephalography; **HFOs,** high-frequency oscillations; **IEDs,** interictal epileptiform discharges; **MRI,** magnetic resonance imaging; **NNMF,** non-negative matrix factorization; **ROC,** receiver operating characteristics

Supplemental digital content is available for this article at www.neurosurgery-online.com.

---

that can coexist or occur independently[1] and are thought to collectively reflect synchronous activity in a hyperconnected epileptic network.[2] To date, their identification in the electroencephalography (EEG) is based on visual recognition of 3 distinctive features: (i) a sudden increase in slope (spikes), (ii) a transient increase in HFOs, and (iii) propagation to neighboring brain areas. Manual interpretation becomes limited and impractical when data increases as a factor of time of recording and number of channels in the setting of chronic high-density intracranial implantation for presurgical workup (>50 electrodes, weeks long). Computer-based EEG-labeling has been investigated for decades and is available with some commercial EEG packages, but often rely on rule-based

TABLE 1. Clinical Summary and Comparison With Machine Detection and Localization

ID	Age sex	Dur	Symptoms	Surgery	Engel outcome	SOZ	IEDs source Clinical	IEDs source Machine	IEDs propagation Clinical	IEDs propagation Machine	IEDs count Machine	Final NNMF rank
EC72	46 M	7	Dyscongnitive Rare SGTCS	R ATL	3 (16 m)	Hpc	Hpc	Hpc	Ent	Ent	6316 (4.4)	4
EC77	44 F	13	Dyscognitive automatism Rare SGTCS	R ATL	2 (14 m)	Parhpc	Parhipc Hpc	Parhpc	Ent	Hpc Ent	3282 (2.3)	5
EC82	65 M	4	Dyscognitive	L ATL	1a (12 m)	Amg	Hpc	Hpc	Ent Fus	Ent Fus	5215 (3.6)	8
EC87	53 F	3	Dyscognitive LUE clonic sz Rare SGTCS	R FLE	2 (12 m)	SFG	OFC$_l$	OFC$_l$	OFC$_m$	OFC$_m$	13686 (9.5)	5
EC91	27 F	3	Experiential Drop attacks Rare SGTCS	L ATL	2 (10 m)	Parhpc	Hpc Amg	Parhpc	Parhpc Cing$_p$	Hpc Amg Cing$_p$	4016 (2.8)	6
EC92	26 M	7	Dyscognitive Dysphasia Automatism SGTCS	L ATL	2 (10 m)	Hpc	Hpc Amg	Hpc Amg	Ent Fus Cing$_a$	Ent Fus Cing$_a$	40882 (28.4)	6

P, patient; Dur, duration; SGTCS, secondarily generalized tonic-clonic seizure; sz, seizure; LUE, left upper extremity; R/L, right/left; ATL, anterior temporal lobectomy; FLE, frontal lobectomy. Engel postoperative class with interval in months (m). SOZ, seizure onset zone. IEDs counts given in total count per 24 h and per min. SFG, superior frontal gyrus; Hpc, hippocampus; Parhpc, parahippocampal cortex; Ent, entorhinal cortex; Cing, cingulate; OFC, orbitofrontal cortices (medial or laterat); Fus, fusiform gyrus; paraHG, parahippocampal gyrus; Ins, insula.

detection (eg, amplitude, slope) and, consequently, the sensitivity and specificity tradeoff is usually poor.[3] The issue of variable IEDs morphology was recently addressed by multitemplate matching, clustering algorithms, and adjustable wavelet analyses,[4–7] but was not extended to the question of patient-specific networks of spike propagation. In contrast, we developed a machine-learning algorithm, based on non-negative matrix factorization (NNMF), that leverages spatiotemporal features across all channels and all time points of 24-h intracranial EEG recordings. Among machine-learning techniques, NNMF performs well with classical problems such as face and speech recognition,[8,9] and recently entered the field of neuroscience as a method to study structural[10] or functional connectivity,[11,12] and recurrent patterns in EEG[13–15] based on the fact that connected regions of the brain covary across a variety of imaging and electrophysiological metrics. Conceptually, NNMF decomposes data into additive constituent representations that can be seen as learned building blocks of the signal.[8] We hypothesized that NNMF could recognize epileptic events from normal physiological data in multichannel EEG. The rationale being that IEDs could be schematically represented as discrete activation of recurring patterns of channel involvement. We found that our algorithm is capable of personalizing to each patient, synthesizing the data into a single anatomic map without human supervision, and detecting and quantifying innumerable IEDs.

METHODS

Subjects and Electroencephalograms

All subjects (n = 6) were medically refractory epilepsy patients implanted for seizure localization; informed consent was obtained and study protocol was approved by the Institutional Review Board. Patients were selected retrospectively to represent a heterogeneous mix of mesiotemporal and neocortical focal epilepsies (Table 1). A 24-h period of continuous EEG (mix of subdural grid, strip, and depth electrodes referenced to a subgaleal electrode) was identified according to (i) at least 48 h postimplant, (ii) minimal number of seizures during that period (if any, ictal discharges were excluded from the analysis).

Algorithm for IED Detection and Localization

See Appendix, **Supplementary Digital Content** for preprocessing, NNMF, and statistical details. As a first step, we used the line-length transform to increase the signal-to-noise ratio of IEDs,[16,17] and output non-negative values that are fit for NNMF (Figure 1). Note that here line-length enhances the "sharpness" of the EEG visible by eye and related to spikes and ripples (80-200 Hz, termed HFOs in this paper; Figure 1). We excluded fast ripples (by bandpass filtering < 200 Hz) because this phenomenon was out of the "pattern recognition" focus of the present methodological development. As a second step, the NNMF algorithm factorizes the line-length transformed data (number of channels × time) into a W matrix (basis functions [BFs] or "bases," number of channels × rank) and an H matrix (activation matrix, rank × time), where the
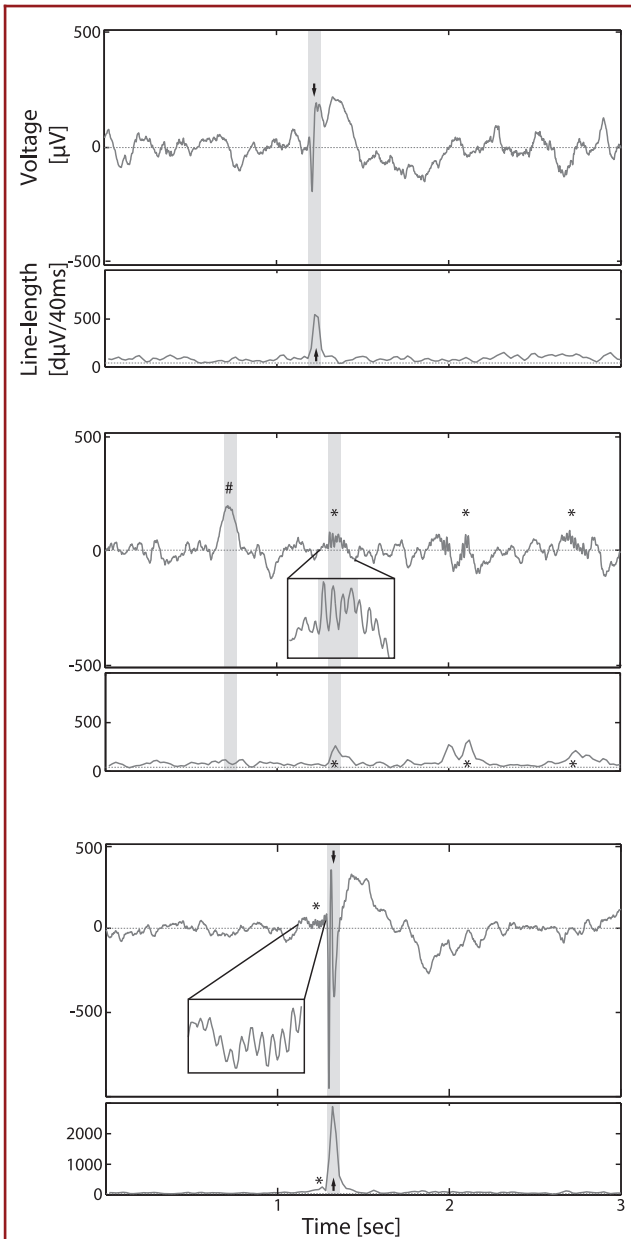
FIGURE 1. *Line-length. Example of EEG (upper panels) and corresponding line-length (lower panels, using 40 ms sliding window) tracing for an amygdala depth electrode in patient 1.* **A**, *Sample of a small epileptic spike (↓) and its after-going slow wave.* **B**, *Sample of 3 successive HFOs (* and inset), note also that a large amplitude slow wave is filtered out by line-length (#).* **C**, *Sample of a large epileptic spike (↓) with preceding HFO (* and inset). Dotted line represents zero for EEG and minimal line-length of 40 µV/40 ms. Note that* **C** *has a different y-axis than* **A** *and* **B** *to accommodate for a very large amplitude spike.*

rank of the decomposition was chosen between 1 and 10 to achieve integration of data in space and time (Figure 2). Given that W and H only have positive entries and that bases are combined only by addition (and not by subtraction), NNMF can intuitively be regarded as a combination of parts (W) to form a whole, where H weights the different parts at each time point.[8] Thresholding the activation vector and the BF of interest detected IEDs in time and space (specific electrodes), respectively. We computed the algorithm's receiver operating characteristics (ROC) against the gold standard of IED marking from 2 neurologists (Y.L.T. and M.O.B.) in 5 of our files. To increase homogeneity in human labeling, the 2 scorers first reached consensus on a few typical discharges labeled by the algorithm (∼20-30 for each file) and then labeled entire raw files independently. To confirm accurate detections, we obtained 5 additional files labeled by 3 neurologists at another hospital. We localized the source of IEDs by projecting the weights found by NNMF on electrode coordinates in a 3-dimensional individual brain reconstruction from the patient's brain magnetic resonance imaging (MRI). To add a temporal dimension to the BFs obtained by NNMF, with a view to infer IED propagation, we applied a convolutive variant of the algorithm.

RESULTS

NNMF Decompositions and IED Detection Accuracy

NNMF found electrode weights corresponding to IEDs and coded for them in one specific BF (W_i; Figure 2); this was consistent across all patients analyzed. Other BFs accounted for lower fluctuations of line-length. The activation vector of interest H_i effectively compressed information for IEDs into a sparse vector (ie, mainly zero-values, except for a few high values at time points with IEDs). Thresholding H_i allowed for the detection of IEDs of variable shape, voltages, and extent but involving a common set of channels. The number of detections over 24 hours varied extensively between patients ranging from 3282 to 40 882 (Table 1).

Comparing machine detections to epileptologist-labeled data sets yielded excellent ROCs (Figure 3) with average sensitivity and specificity of 93% and 97%, respectively. This was also true for training and labeling on recordings of only 10-min length, but the sensitivity went down with shorter training sets (**Table**, **Supplemental Digital Content 2**, rows 1 and 2). Training BFs on 24-h recording and applying them to test data always yielded excellent results (**Table**, **Supplemental Digital Content 2**, rows 3-5). Our method for setting the detection threshold (see Methods) yielded an optimal sensitivity and specificity tradeoff (ie, the threshold was at the elbow of the ROC). Cohen's kappa agreement (interrater reliability) was substantial (kappa > 0.6) to almost perfect (kappa > 0.8) both among human scorers and with the machine, validating the ROC reported here. In addition, we confirmed excellent agreement with data labeled independently by epileptologists not involved in the present study (**Table**, **Supplemental Digital Content 3**).
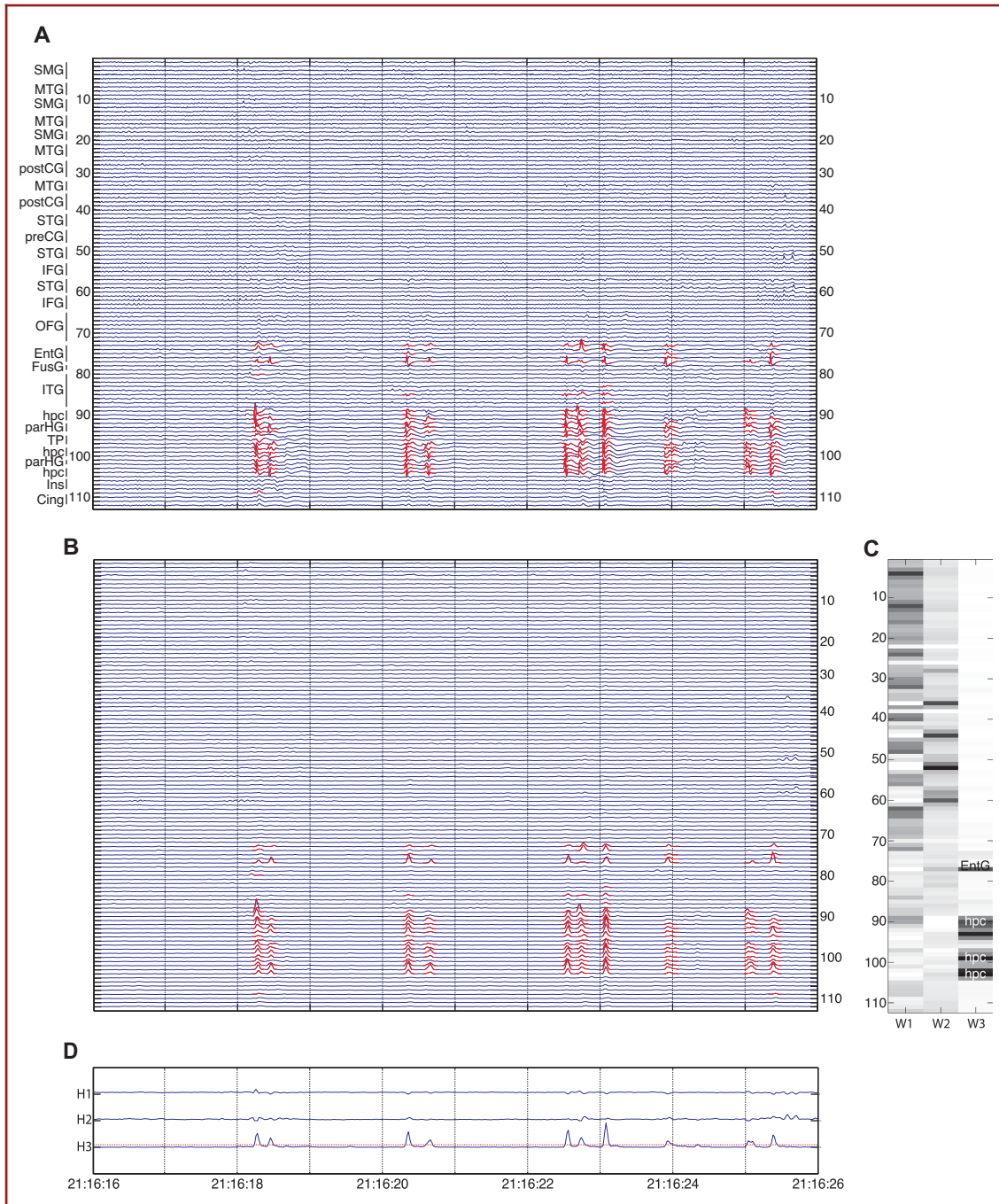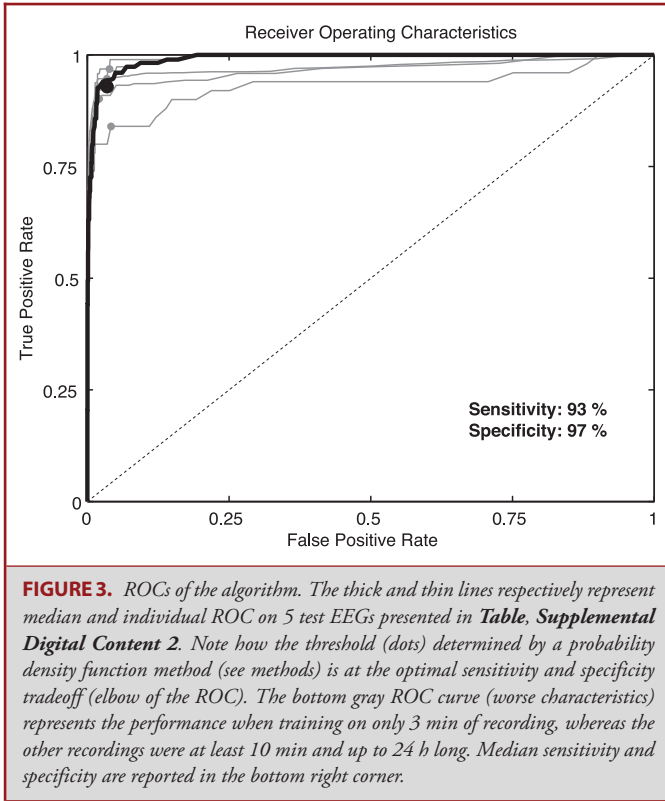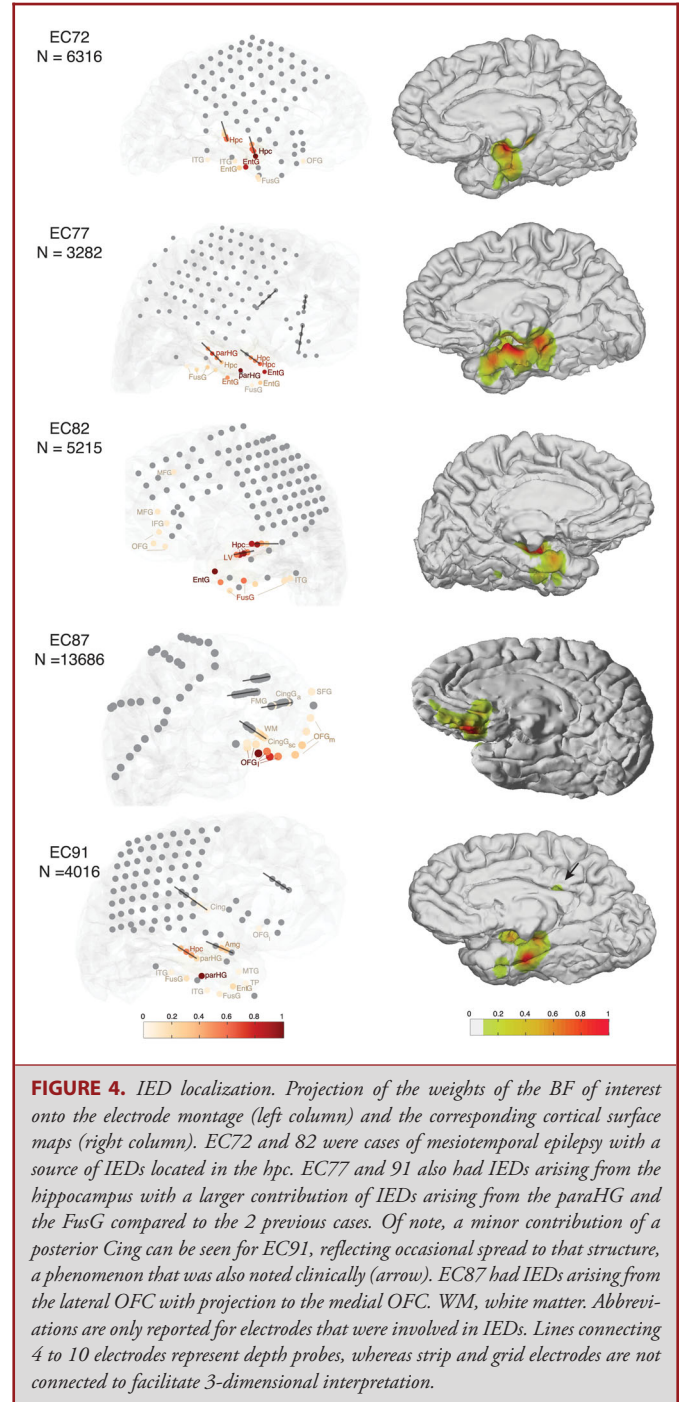
FIGURE 2. *Decomposition. Two-step detection algorithm using line-length transform and NNMF decomposition.* **A**, *Sample preprocessed 112 channel EEG over 10 s extracted from 24-h recording in patient EC92 showing 10 IEDs of slightly varying topography and amplitude.* **B**, *Line-length transform.* **C**, *NNMF BFs. Note how W_3 calculated on 24 h of data summarizes the set of channels commonly involved in all IEDs shown here. Gray-scale represents individual electrode weights (arbitrary units, darker corresponds to stronger weight).* **D**, *NNMF activation matrix. H_3 accurately compresses the information in space into a single dimension (instead of more than 15 channels that have IEDs). Red dotted line: threshold for detections. In this representative case, IEDs involved mostly the hippocampus (Hpc) and the entorhinal cortex (EntG) but also propagated with a mild delay to the cingulate (Cing) and orbitofrontal cortices (OFC). Interestingly, W_2 has activation weights every eighth channel, which corresponds to the posterior electrodes on the hemispheric grid and reflects the posterior dominant rhythm. STG, MTG, ITG: superior, middle, and inferior temporal gyrus. SMG, supra-marginal gyrus. Pre, post CG: central gyrus; SFG, MFG, IFG: superior, middle, and inferior frontal gyri; FusG: fusiform gyrus; paraHG: parahippocampal gyrus; Ins: insula.*

FIGURE 3. *ROCs of the algorithm. The thick and thin lines respectively represent median and individual ROC on 5 test EEGs presented in* **Table**, **Supplemental Digital Content 2**. *Note how the threshold (dots) determined by a probability density function method (see methods) is at the optimal sensitivity and specificity tradeoff (elbow of the ROC). The bottom gray ROC curve (worse characteristics) represents the performance when training on only 3 min of recording, whereas the other recordings were at least 10 min and up to 24 h long. Median sensitivity and specificity are reported in the bottom right corner.*
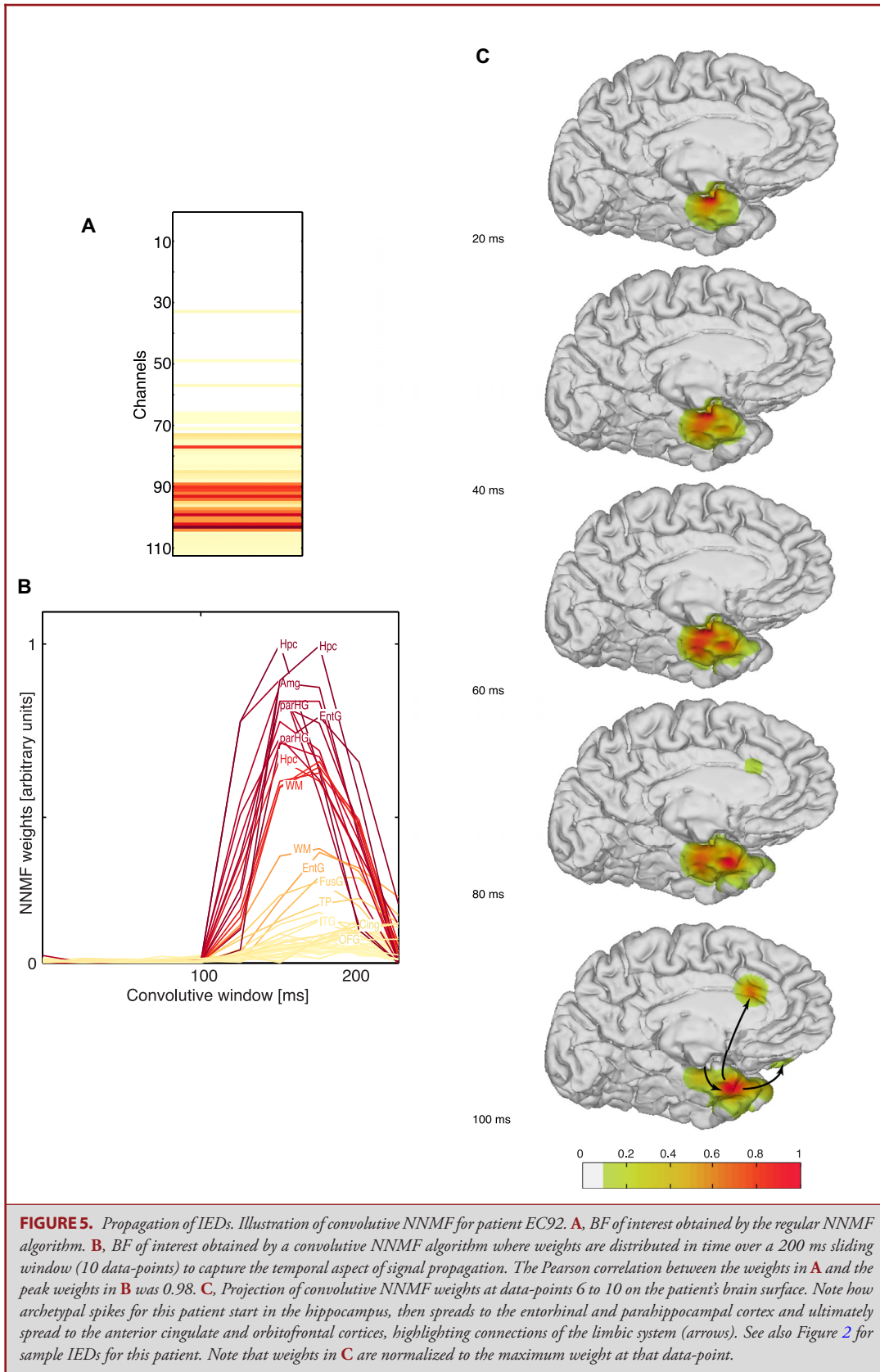
IED Localization

Projected weights of W_i onto the brains of patients 1 to 5 (Figure 4) resulted in a summary map of 24-h recordings taking into account every detected IED. An electrode that has a high weight is an electrode that contributed large voltage changes or frequents IEDs. Conversely, an electrode that has a low weight (but still above the mean of W_i, per our definition) is only occasionally involved in extensive spikes or only has small voltage changes when included. Indeed, in a linear regression model including 2 predictors, NNMF BFs weights were explained at 90% (adjusted R^2) mostly by the frequency of involvement of the corresponding channel (coefficient = 0.3, $P < .001$) with a minor contribution of the average line-length of IEDs in that same channel that was not independent from the frequency of involvement (coefficient = 0.0006, $P < .001$ for the interaction term, no significant coefficient for mean line-length alone). Comparison to the localization of IEDs documented in the daily clinical EEG reports is shown in Table 1. As one can see, machine-learning identified the parahippocampal cortex in patient EC77 and EC91 as the IEDs onset zone, whereas it was identified as the site of propagation by clinicians. When using convolutive NNMF, peak weights were identical to those found by regular NNMF (patient 6, correlation 0.98, $P < .001$) but their ascent and descent was staggered in time for channels successively activated. Projected weights of W_i onto the brain reconstruction

FIGURE 4. *IED localization. Projection of the weights of the BF of interest onto the electrode montage (left column) and the corresponding cortical surface maps (right column). EC72 and 82 were cases of mesiotemporal epilepsy with a source of IEDs located in the hpc. EC77 and 91 also had IEDs arising from the hippocampus with a larger contribution of IEDs arising from the paraHG and the FusG compared to the 2 previous cases. Of note, a minor contribution of a posterior Cing can be seen for EC91, reflecting occasional spread to that structure, a phenomenon that was also noted clinically (arrow). EC87 had IEDs arising from the lateral OFC with projection to the medial OFC. WM, white matter. Abbreviations are only reported for electrodes that were involved in IEDs. Lines connecting 4 to 10 electrodes represent depth probes, whereas strip and grid electrodes are not connected to facilitate 3-dimensional interpretation.*

revealed the successive activation of structures of the limbic circuit (Figure 5).

Rank of Decomposition

As expected for the NNMF algorithm, the total explained variance increased monotonically, as the rank increased (**Figure**,

FIGURE 5. *Propagation of IEDs. Illustration of convolutive NNMF for patient EC92.* **A**, *BF of interest obtained by the regular NNMF algorithm.* **B**, *BF of interest obtained by a convolutive NNMF algorithm where weights are distributed in time over a 200 ms sliding window (10 data-points) to capture the temporal aspect of signal propagation. The Pearson correlation between the weights in* **A** *and the peak weights in* **B** *was 0.98.* **C**, *Projection of convolutive NNMF weights at data-points 6 to 10 on the patient's brain surface. Note how archetypal spikes for this patient start in the hippocampus, then spreads to the entorhinal and parahippocampal cortex and ultimately spread to the anterior cingulate and orbitofrontal cortices, highlighting connections of the limbic system (arrows). See also Figure 2 for sample IEDs for this patient. Note that weights in* **C** *are normalized to the maximum weight at that data-point.*

Supplemental Digital Content 4). The optimal rank used for IED localization varied from patient to patient ranging from 4 to 8 (**Table, Supplemental Digital Content 2**). Since no principled way is established to select the optimal rank beforehand, we explored the stability of our results through a series of decompositions across increasing ranks. We found that low ranks (eg, rank of 2) yielded BFs coding for pathological signal but also background fluctuation given their need to optimally explain the total variance. Generally, the BF of interest was quite well defined at a rank of 4 or above. The average correlation among BFs of interest was 0.81 ± 0.16 ($P < .001$) from rank 2 to 10 and 0.97 ± 0.04 ($P < .001$) at and above the optimal rank defined individually (see Methods). The percent of variance explained by W_i and H_i alone reflected the same trend as it decreased across low ranks (eg, ranks of 2 to 4) and stabilized at a lower value above the individual optimal rank. This means that W_i initially gains in specificity (explaining less of the total variance) and stabilizes beyond a minimal rank (eg, 4) to explain only and entirely the pathological data.

DISCUSSION

Here, we showed that statistical learning by NNMF could derive distinct pathological features of an intracranial EEG. When inspecting representations used by the NNMF algorithm to detect abnormal activity, we found that it attributed weights to electrodes that reflected their involvement in IEDs. By drawing from hours of recordings at a time and finding the common feature of all detected IEDs across the circadian cycle, this method statistically synthesizes innumerable data and makes it intelligible to the clinician in the form of a single localization map representing the archetypal IED for a specific patient. The addition of a convolutive window to the algorithm enables the study of the circuits of propagation of IEDs.[18,19] This is in contrast with other matrix factorization techniques such as principal or independent component analyses where the result often lacks intuitive interpretability. Another key advantage of NNMF is that it is fully unsupervised, meaning that the machine learns merely by the recurrence of patterns in unlabeled data. This is contrary to neural networks that require training through exposure to a quantity of prelabeled data.[20] Unlike previous applications of NNMF to the EEG spectral domain that can capture task-related oscillations,[13,14] we focused on best-defined temporal features of IEDs with further emphasis on their spatial distribution. Because focal epilepsies are patient-specific, we did not endeavor to look for common patterns across patients using NNMF,[13] but this could be feasible across a larger cohort.

Furthermore, we showed that the algorithm developed here has an excellent sensitivity and specificity tradeoff that seems similar or superior to algorithms developed elsewhere,[4,21] including head-to-head comparison on identical data.[22] Our algorithm is resistant to false positives by nature. For example, a spurious increase in slope in an isolated channel would lack the activation of the entire base and would thus be skipped or included in separate bases if a larger rank is used. Conversely, it is also highly sensitive to minor changes involving a set of channels similar to the base of interest, thereby detecting IEDs despite some level of variability in morphology from one to the next. We showed that bases found by NNMF are stable for a given patient across ranks of decomposition, meaning that the derived solution is robust and immune to small changes in the parameters of the algorithm. Although performance of the algorithm tends to increase with more data, we showed that it agreed with human labeling even on 5-min recordings. One setting where it may fail is if only one example of a discharge is present in a very long recording, but this is a rare clinical situation with intracranial EEG.

Highly reliable tools for localization-related epilepsy are critical, as the success of resective surgery depends on precise determination of the epileptogenic zone. EEG-based spatial localization (eg, source imaging) remains a critical tool as it was shown to be superior to advanced and expensive neuroimaging techniques such as MRI, positron emission tomography, and single-photon emission computed tomography techniques.[23] Manual ranking of the channels most often involved in IEDs (and thus the anatomic location) can vary extensively from one scorer to the next.[24] We found that NNMF attributed weights to channels resulting from a linear combination of their frequency of involvement in IEDs and the average IED line-length. Overall, the method seems closer to visual pattern recognition used by human observers than a combination of rules on single dimension metrics (ie, single channel detections), offering a key spatial integrative advantage. This has conceptual and practical implications: the core of the algorithm relies on the existence of an IED's onset zone and extended propagation zone(s) and in doing so, it quantifies the localization of the irritative tissue, which is of clinical value for epilepsy surgery. Thus, our algorithm exploits spatial integration and adds temporal integration. At the millisecond level, we showed that line-length temporally integrates different types of IEDs including spikes and HFOs into a single metric, placing greater emphasis on sharp elements of the EEG compared to physiological background. At the subsecond level, the use of convolutive NNMF provided additive information about the networks of IEDs propagation. This could be valuable for detecting subtle intricacies of broader epileptic networks that could likely add clinical relevance. At the level of a full 24-h cycle, temporal integration was possible as well, as line-length can be down-sampled and large files can be processed by NNMF. Processing data over the entire circadian cycle offers an opportunity to capture the epileptic brain in all vigilance states, which is important when considering IEDs such as HFOs that are more prominent during sleep.[25] Given that isolated HFOs occur more rarely than interictal spikes, it is likely that their contribution to the BFs found here was inferior to spikes. However, NNMF weights reflect an unbiased distribution of these 2 events through the lens of line-length. Spikes with overriding HFOs are potentially as relevant to localization as isolated HFOs[1] and were also represented with our method. The goal here was to obtain a

single summary map, but if HFOs were to be confirmed as better markers of the epileptogenic zone than spikes, the algorithm could be adjusted to detect only HFOs by prefiltering/bandpassing before the calculation of line-length. Seizures were not included in the present analyses but adjusting windows to achieve temporal integration at a larger scale (eg, 5 s) could enable the use of a similar method for their detection. Although we demonstrated consistency with clinical reports of the IED foci, larger scale studies comparing NNMF-based localization to surgical outcome data in more subjects will be necessary to confirm its true clinical value.

CONCLUSION

In summary, applying NNMF to the detection of IEDs engenders multiple important and novel features. This method is automatic and unsupervised (therefore time-saving), and is one of the few detection algorithms that learns an individual's unique IEDs and captures its archetype, which is of value in surgical planning. It is also quantitative, counting beyond what is practical by manual methods and is applicable to long time-scales, such as multiple days in the epilepsy monitoring unit, and potentially months/years of data with portable intracranial EEG.[26] Potential future applications include characterization of long time-scale IEDs rhythms (eg, circadian), which could guide anti-epileptic drug dosing and timing. Machine-detected IEDs may serve as a biomarker for the effectiveness of medications[27] or neurostimulation.[28] Intraoperative guidance of epilepsy surgery using IEDs is currently under investigation[29] and algorithms such as ours may accelerate the interpretability of such recordings. Characterizing the localization specificity of epileptiform discharges of a given patient may be a prerequisite for future closed loop devices, where a set of prelearned bases could significantly accelerate computations for the detection of subsequent similar discharges in real time. We anticipate that our study is a step forward for machine-learning in clinical neurophysiology. These computational technologies have had a tremendous success in nonmedical fields and may soon become routine aids to the neurosurgeon and neurologist.

Disclosures

REFERENCES

1. Ren L, Kucewicz MT, Cimbalnik J, et al. Gamma oscillations precede interictal epileptiform spikes in the seizure onset zone. *Neurology*. 2015;84(6):602-608.
2. Rao VR, Lowenstein DH. Epilepsy. *Curr Biol*. 2015;25(17):R742-R746.
3. Ver Hoef L, Elgavish R, Knowlton RC. Effect of detection parameters on automated electroencephalography spike detection sensitivity and false-positive rate. *J Clin Neurophysiol*. 2010;27(1):12-16.
4. Lodder SS, Askamp J, van Putten MJ. Inter-ictal spike detection using a database of smart templates. *Clin Neurophysiol*. 2013;124(12):2328-2335.
5. Chavakula V, Sánchez Fernández I, Peters JM, et al. Automated quantification of spikes. *Epilepsy Behav*. 2013;26(2):143-152.
6. Nonclercq A, Foulon M, Verheulpen D, et al. Cluster-based spike detection algorithm adapts to interpatient and intrapatient variation in spike morphology. *J Neurosci Methods*. 2012;210(2):259-265.
7. Horak PC, Meisenhelter S, Testorf ME, Connolly AC, Davis KA, Jobst BC. Implementation and evaluation of an interictal spike detector. Bones PJ, Fiddy MA, Millane RP, eds. *SPIE Optical Engineering + Applications*. Proc. SPIE. 2015;9600:96000N1-96000N11, doi:10.1117/12.2189248.
8. Lee DD, Seung HS. Learning the parts of objects by non-negative matrix factorization. *Nature*. 1999;401(6755):788-791.
9. Smaragdis P. Convolutive speech bases and their application to supervised speech separation. *IEEE T Audio Speech*. 2007;15(1):1-12.
10. Sotiras A, Resnick SM, Davatzikos C. Finding imaging patterns of structural covariance via non-negative matrix factorization. *Neuroimage*. 2015;108:1-16.
11. Wei J, Bai W, Liu T, Tian X. Functional connectivity changes during a working memory task in rat via NMF analysis. *Front Behav Neurosci*. 2015;9(11):e17. doi:10.3389/fnbeh.2015.00002.
12. Shokrollahi M, Krishnan S. Non-negative matrix factorization and sparse representation for sleep signal classification. *Conf Proc IEEE Eng Med Biol Soc*. 2013:4318-4321. doi:10.1109/EMBC.2013.6610501.
13. Lee H, Choi S. Group non-negative matrix factorization for EEG classification. *AISTATS*. 2009;5:320-327.
14. Lee H, Cichocki A, Choi S. Kernel nonnegative matrix factorization for spectral EEG feature extraction. *Neurocomputing*. 2009;72(13-15):3182-3190.
15. Wen D, Jia P, Lian Q, Zhou Y, Lu C. Review of sparse representation-based classification methods on EEG signal processing for epilepsy detection, brain-computer interface and cognitive impairment. *Front Aging Neurosci*. 2016;8:172. doi:10.3389/fnagi.2016.00172.
16. Bergstrom RA, Choi JH, Manduca A, Shin HS, Worrell GA, Howe CL. Automated identification of multiple seizure-related and interictal epileptiform event types in the EEG of mice. *Sci Rep*. 2013;1483. doi:10.1038/srep01483.
17. Esteller R, Echauz J, Tcheng T. Comparison of line length feature before and after brain electrical stimulation in epileptic patients. *Conf Proc IEEE Eng Med Biol Soc*. 2004;7:4710-4713. doi:10.1109/IEMBS.2004.1404304.
18. Bourien J, Bartolomei F, Bellanger JJ, Gavaret M, Chauvel P, Wendling F. A method to identify reproducible subsets of co-activated structures during interictal spikes. Application to intracerebral EEG in temporal lobe epilepsy. *Clin Neurophysiol*. 2005;116(2):443-455.
19. Coito A, Plomp G, Genetti M, et al. Dynamic directed interictal connectivity in left and right temporal lobe epilepsy. *Epilepsia*. 2015;56(2):207-217.
20. Halford JJ, Schalkoff RJ, Zhou J, et al. Standardized database development for EEG epileptiform transient detection: EEGnet scoring system and machine learning analysis. *J Neurosci Methods*. 2013;212(2):308-316.
21. Barkmeier DT, Shah AK, Flanagan D, et al. High inter-reviewer variability of spike detection on intracranial EEG addressed by an automated multi-channel algorithm. *Clin Neurophysiol*. 2012;123(6):1088-1095.
22. Janca R, Jezdik P, Cmejla R, et al. Detection of interictal epileptiform discharges using signal envelope distribution modelling: application to epileptic and non-epileptic intracranial recordings. *Brain Topogr*. 2015;28(1):172-183.
23. Brodbeck V, Spinelli L, Lascano AM, et al. Electroencephalographic source imaging: a prospective study of 152 operated epileptic patients. *Brain*. 2011;134(pt 10):2887-2897.
24. Barkmeier DT, Shah AK, Flanagan D, et al. High inter-reviewer variability of spike detection on intracranial EEG addressed by an automated multi-channel algorithm. *Clin Neurophysiol*. 2012;123(6):1088-1095.
25. Jacobs J, Staba R, Asano E, et al. High-frequency oscillations (HFOs) in clinical epilepsy. *Prog Neurobiol*. 2012;98(3):302-315.
26. Bergey GK, Morrell MJ, Mizrahi EM, et al. Long-term treatment with responsive brain stimulation in adults with refractory partial seizures. *Neurology*. 2015;84(8):810-817.
27. Zijlmans M, Jacobs J, Zelmann R, Dubeau F, Gotman J. High-frequency oscillations mirror disease activity in patients with epilepsy. *Neurology*. 2009;72(11):979-986.
28. Heck CN, King-Stephens D, Massey AD, et al. Two-year seizure reduction in adults with medically intractable partial onset epilepsy treated with responsive

neurostimulation: final results of the RNS System Pivotal trial. *Epilepsia.* 2014;55(3):432-441.

29. van't Klooster MA, Leijten FS, Huiskamp G, et al. High frequency oscillations in the intra-operative ECoG to guide epilepsy surgery ("The HFO Trial"): study protocol for a randomized controlled trial. *Trials.* 2015;16(1):422. doi:10.1186/s13063-015-0932-6.

***Supplemental digital content** is available for this article at www. neurosurgery-online.com.*

Acknowledgments